

The Effects of Source on the Generation of Short Period Surface Waves

YEONG TEIN YEH¹ and JEN-KUANG CHUNG^{1,2}

(Manuscript received 14 September 1993, in final form 3 December 1993)

ABSTRACT

Short-period surface waves can usually be observed on strong motion records. Theoretical seismograms provide a useful tool for the prediction and interpretation of differences in the surface wave excitation of various earthquakes. The complex polarization filter followed by Vidale (1986) is used in this paper. The influence of source parameters (source depth, source type and orientation) on the excitation of Rayleigh waves for the elastic half-space and a single layered half-space model is discussed in detail.

Results show that the epicentral distance beyond which the fundamental mode Rayleigh waves can be generated is around 3 to 5 times of the source depth for the point dislocation source in the half-space model. These critical distances are a little longer than those for the finite length sources. The orientation parameter is not generally of significance. When a flat low-velocity layer is overlying on the top of the half-space, the computations suggest that the complex waveforms are observed and about 10 km of the critical distance obtained is not changed for all kinds of sources used in this study. Moreover, the most important quantity for identifying the Rayleigh wave, namely the ellipticity, is estimated to be in the range of 0.6 to 0.7, except with a layer over half-space model.

1. INTRODUCTION

In the period of the 1960's and 1970's, seismologists investigated the Earth's crust-upper mantle structures using the dispersive characteristics of surface waves (e.g. Dorman *et al.*, 1960; Knopoff, 1972). Progress has since been further accomplished with the higher quality data recorded from dense advanced seismometers and the development of computer facilities which enable more precise statements on local structure. Therefore, numerous papers are focused on the behaviors of short-period surface waves (Kafka and Dollin, 1985; Yao and Dorman, 1992), concerning the recent popularly discussed site responses.

¹ Institute of Earth Sciences, Academia Sinica, P.O. Box 1-55, Nankang, Taipei, Taiwan, R.O.C.

² Central Weather Bureau, 64, Kung Yuan Road, Taipei, Taiwan, R.O.C.

It has been recognized for some time that damage during earthquakes is often caused by significant amplification of seismic ground motions near the Earth's surface sedimentary deposits with very low shear rigidity (Hong and Helmberger, 1978). The most noticeable recent examples were the severe damages observed in the lake-bed zone of Mexico City during the Michoacan Earthquake of 19, September 1985 (e.g. Singh *et al.*, 1988; Campillo *et al.*, 1989) and in the San Francisco Bay area during the 17, October 1989 Loma Prieta Earthquake (Hough *et al.*, 1990; Hanks and Brady, 1991). Besides the large amplitude observed in these cases, the long-lasting duration could essentially be composed of the resonant modes excited by the geometry-dependent enclosed basins (Bonamassa and Vidale, 1991; Rial and Ling, 1992) and the basin-induced surface waves (Bard *et al.*, 1988).

The generation of surface waves is mainly controlled by the near-surface structure in the Earth which traps the seismic energy within it (Keilis-Borok, 1989). Surface waves generated by conversion of incident body waves at the basin edge were investigated by Bard and Bouchon (1980). Phillips *et al.* (1993) also showed that the 1-sec Love waves emanate from a short segment of the Kanto basin boundary for a wide distribution of earthquakes in Japan. However, the other important purpose of analyzing the surface waves is to inverse source parameters making use of different approaches (Mendiguren, 1977; Kanamori and Given, 1981; Yan and Alexander, 1990). Most of their studies were based on relatively far-field observations. Up to now, as is well understood the generation of near-source surface waves has yet to be discussed in great detail. In order to isolate the source term from the path and structure effects, this study numerically simulates the simplest available environments for developing surface waves by using the polarization characteristics of particle motions.

Different from earlier studies (Sexton *et al.*, 1977; Wang and Wu, 1989), these researchers estimate the ellipticity of particle trajectory by tracing the wavelet spreading from source on the two-dimensional space, to determine the surface wave generating distance under different source patterns. This procedure, in turn, may provide some ideas on the problem of structural inversion on the interpretation of seismograms.

2. METHOD

It has been understood for a long time that body waves and surface waves exhibit distinct polarization in an elastic medium (Bath, 1973). Many techniques of polarization analysis were proposed (e.g. Montalbetti and Kanasevich, 1970; Vidale, 1986; Shieh and Herrmann, 1990). The special importance attached to elliptic and linear polarization is not due to the mere fact that these are simple to study. In fact, the velocities of elastic waves in the Earth are intimately related to their polarization. For this reason the division of a record into waves based on their typical velocities is largely equivalent to the division into signals whose polarization vectors are weakly dependent on frequency (Keilis-Borok, 1989).

2.1 Numerical Modeling

With the purpose of modeling complex sources and heterogeneous structures, a finite element method was chosen to formulate the elastic wave equation. Partially following some of the ready-made subroutines (Smith, 1982), these researchers used the finite element computer code developed by Huang (1988) in the present study. It effectively eliminates numerical reflections from the artificial boundaries using the absorbing boundary skill proposed by Smith (1974), and involves the split node technique (Melosh and Raefsky, 1981) for simulating dislocation sources.

Two essential conditions, i.e. the wider model and longer duration of calculation, are practically necessary for the growing up of surface waves. The model is 150 km long in the horizontal direction and 50 km deep in the vertical direction so as to avoid the higher-order unwanted reflections that, in fact, the employed analytical formulation cannot eliminate. The single element size is 1 km square. As a result, the seismic waves in the wavelength range of between 5 and 10 km will be passed by the numerical mesh.

As the matrix differential full-wave equation is implemented and solved in the time domain using the central difference method, the solution undoubtedly includes near-field and far-field terms. The synthetic seismogram on each node is then calculated and stored selectively for further analysis. It is also beneficial to obtain sequential displacement snapshots of simultaneously equal time intervals. The aspects of the propagating waves are then easily revealed in the way of a colored cartoon displayed on a computer screen. The behaviors of seismic waves in the near-source region are likely to be complicated and difficult to interpret before they convert to surface waves. At the same time, the waveforms on every certain depth are therefore plotted together to trace the target wavelet and to estimate its apparent horizontal velocity. It is necessary to be very careful to pick the correct phase (Figure 1). The procedures used here are helpful in distinguishing wave types.

The spatial variation of the amplitude and period of seismic waves can cautiously be observed although it's not the subject of the study here. However, this does demonstrate that most of the energy is trapped within the top layer or near free surface during the propagation of surface waves (Figure 2). Therefore, the polarization parameters are calculated only on the section 30 km long and 10 km thick from free surface (the block enclosed by dashed lines in Figure 2).

2.2 Identification of Surface Waves

The complex polarization analysis (Vidale, 1986) was undertaken to estimate the polarization properties of synthesized particle motion in this study. In the case of three-component signal, three time series, $U_r(t)$ for the radial component, $V_r(t)$ for the tangential component, and $W_r(t)$ for the vertical component, are converted to an analytic signal

$$\begin{aligned} U(t) &= U_r(t) + iH(U_r(t)) \\ V(t) &= V_r(t) + iH(V_r(t)) \\ W(t) &= W_r(t) + iH(W_r(t)) \end{aligned} \quad (1)$$

where H represents the Hilbert transform, and i is $\sqrt{-1}$.

The analytic signal may be used to compute the covariance matrix

$$C(t) = \begin{pmatrix} UU^* & UV^* & UW^* \\ VU^* & VV^* & VW^* \\ WU^* & WV^* & WW^* \end{pmatrix} \quad (2)$$

where the asteriske (*) represents complex conjugation. Then, the three eigenvalues λ_i and eigenvectors (x_i, y_i, z_i) of the matrix may be obtained by solving the equations.

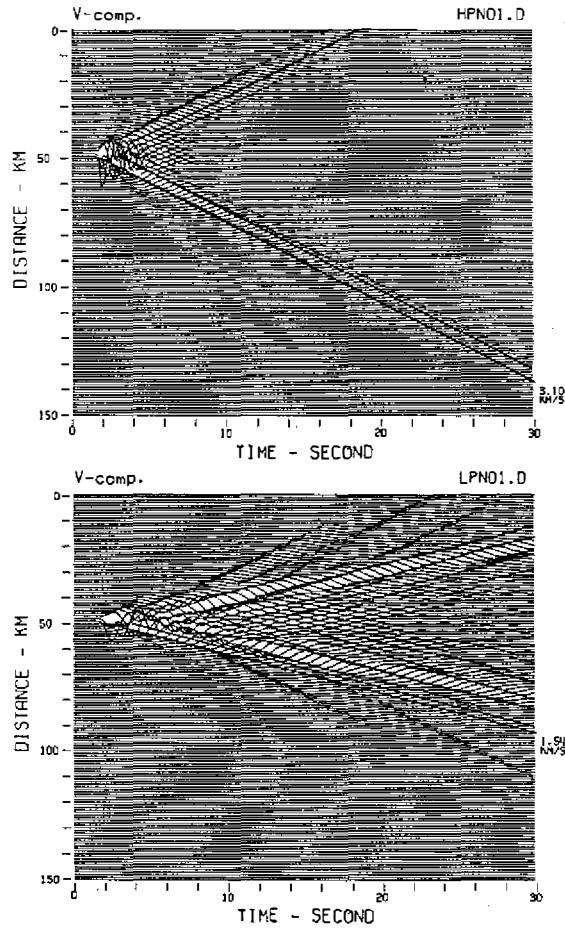


Fig. 1. Synthetic seismograms at free surface of half-space model (upper) and a layer over half-space model (lower) for a point dislocation source located at 2 km in depth. The waveform within broad lines are analyzed.

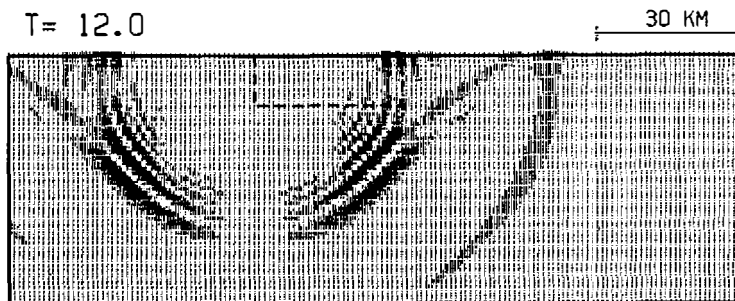


Fig. 2. The snapshot of the seismic waves emanating from a point dislocation source located at 2 km in depth in the half-space finite element model.

$$\begin{pmatrix} x_i \\ y_i \\ z_i \end{pmatrix} (C - \lambda_i I) = 0, \quad i = 1, 2, 3. \tag{3}$$

where I is a 3 by 3 unit matrix. The eigenvector (x_0, y_0, z_0) associated with the largest eigenvalue λ_0 represents the direction of the largest amount of polarization. However, the phase in the complex plane of the eigenvectors is unknown. Therefore, the eigenvector associated with the largest eigenvalue must be rotated by an angle α in the complex plane, to find the maxima length of the real component of the eigenvector, i.e. to maximize

$$X = \sqrt{(Re(x_0 A))^2 + (Re(y_0 A))^2 + (Re(z_0 A))^2} \tag{4}$$

where A is $\cos \alpha + i \sin \alpha$ and $Re(x)$ is the real part of x . The elliptical component of polarization (also called ellipticity) may be estimated by

$$P_E = \frac{\sqrt{1 - X^2}}{X} \tag{5}$$

P_E is 0° for linearly polarized motion. In contrast, P_E is 1 for circularly polarized motion. The strike (ϕ) and dip (δ) of the direction of maximum polarization are

$$\phi = \tan^{-1} \left(\frac{Re(y_0)}{Re(x_0)} \right), \quad -90^\circ \leq \phi \leq 90^\circ \tag{6}$$

$$\delta = \tan^{-1} \left(\frac{Re(z_0)}{\sqrt{Re(x_0)^2 + Re(y_0)^2}} \right), \quad -90^\circ \leq \delta \leq 90^\circ \tag{7}$$

By definition, 0° both in strike and dip represents a vector which points horizontally in the direction toward the epicenter.

Simplification of the polarization method to two components is straightforward and has been examined by synthetic sinusoidal waveforms. The polarization characteristics estimated by applying this method almost match the theoretical values. The covariance may be smoothed over a running window to provide more stable estimates. But this procedure will result in decreasing the time resolution in compensation. These authors suggest the width of the moving window might be about half of the predominant period of synthesized surface waves.

Therefore, the time variant covariance matrix (equation (2)) of each node for the mentioned profile is averaged individually over a 1 second wide moving window, i.e. 10 times the sampling interval, and overlapping one sampling interval to suppress the numerical instability. Finally, the averages of the ellipticity defined by equation (5) over the selected wavelet (i.e. the interval between two paralleled dashed lines shown in Figure 3) for each node are estimated and expressed as the contour diagrams. These figures represent the variation of the ellipticity of particle motion for certain wavelets propagating through the different positions of the two-dimensional medium.

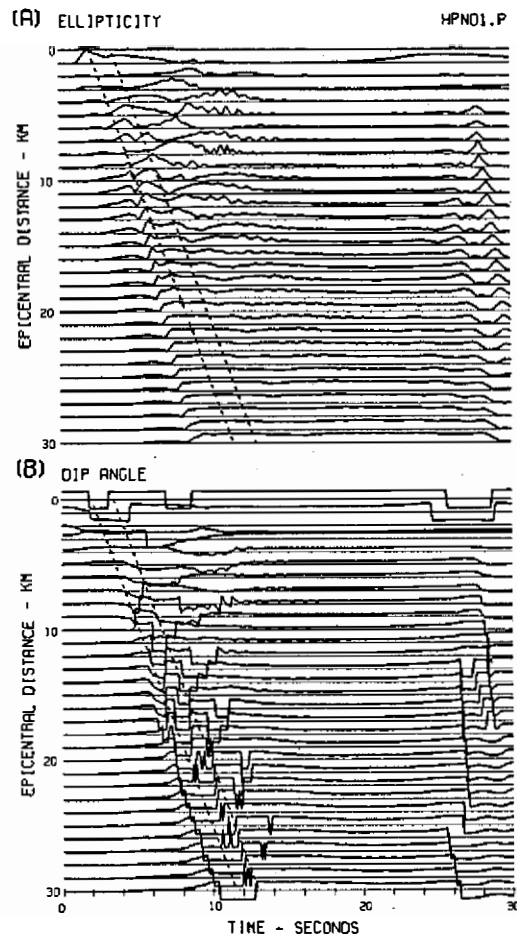


Fig. 3. For the case of the half-space model and source excited at 2 km in depth, (A) ellipticity - time and (B) dip angle of polarization - time relations derived from the theoretical seismograms on surface receivers. The intervals between the dashed lines are the time window used for calculating average polarization parameters.

3. RESULTS AND DISCUSSION

In order to investigate the distance for generating distinct Rayleigh waves controlled by different sources, two simplified crustal models of the half-space and a layer over half-space were considered (Figure 4). Both the bedrock and sediment are homogeneous and isotropic. These are the simplest models in which Rayleigh waves can exist and propagate definitively.

A source time function of the Gaussian pulse with an amplitude decay factor of 50 and a dominant period of 0.6 second is used in all cases. The idealized dislocation sources are modeled as normal faults with individual dip angles of 26° , 45° and 63° . In addition to the point source, the finite source with about a length of 3 km is also considered. The downgoing

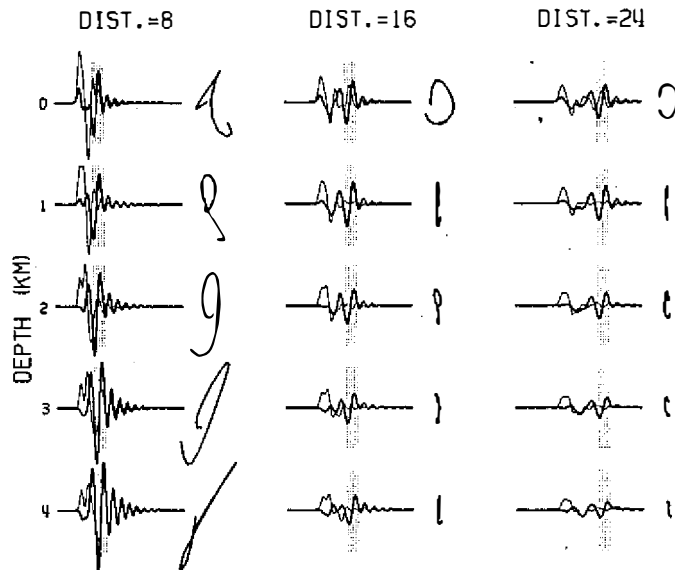


Fig. 5. Synthetic seismograms and particle motions corresponding to the shadow block of 1.5 sec wide. Broad and thin lines represent vertical and horizontal components respectively. All of the seismograms are plotted to the same scale.

5 derived by the Cagniard-de Hoop method (Aki and Richards, 1980, p.240). The discrepancy is caused by the difference in defining the critical distance, which is defined as the epicentral distance in this study but as the source to receiver distance in their formula. Another reason for the smaller ratio here is that the critical distances are decided on the diagrams like Figure 6 and 7 by identifying where the definite, not well-developed, Rayleigh wave begins to build up. The variation of ellipticity on the free surface (Figure 8 (a)) can interpret this relationship.

When a selected wavelet propagates below the free surface, one obvious trend of elliptic-polarization with a dip angle of about 30° is observed for each case of different source depth. This is the result of the SV-predominant wavelet contaminated by the reflected pS and SP phases. Another phenomenon is also due to the particle motions exhibiting very complex behaviors near the source, especially for the deeper source cases.

With a change in the source to a 3 km in length normal fault with a dip angle of 45° , the results introduce the shorter critical distances of 7 km, 10 km, 12 km, and 16 km respectively (Figure 7 and 8 (b)), compared with the previous point sources. The chaos in the vicinity of source region still exist and the elliptic polarization trends are no longer evident because of the superposition of the latter SV-predominant arrivals emanating from the propagating rupture to maintain the linear polarized motion at such an angle. In rotating the dip angle of the finite fault to 26° or 63° , the critical distances do not show significant changes except with the two deeper source cases (Figure 8 (c) and 8 (d)).

An interesting phenomenon must be mentioned here which is that the ellipticity of the wavelet passing on the free surface changes with a periodic fluctuation before it reaches a stable value say in the range of 0.6 to 0.7. The cases of point source (Figure 8 (a)) especially

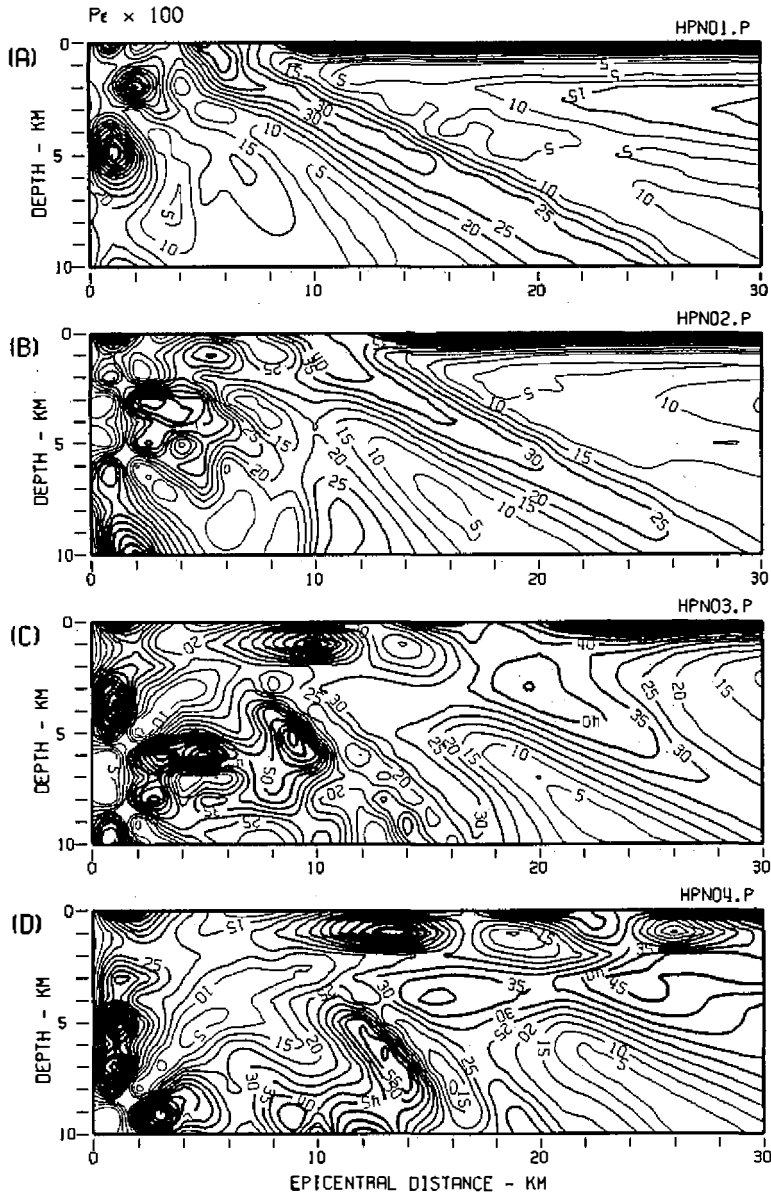


Fig. 6. The averaged ellipticity variations of particle motions over space for certain wavelet propagating through the different positions of the two-dimensional half-space medium. These diagrams are for (A) 2 km, (B) 4 km, (C) 7 km, and (D) 10 km of point source depths respectively. The contour values shown are 100 times the ellipticities.

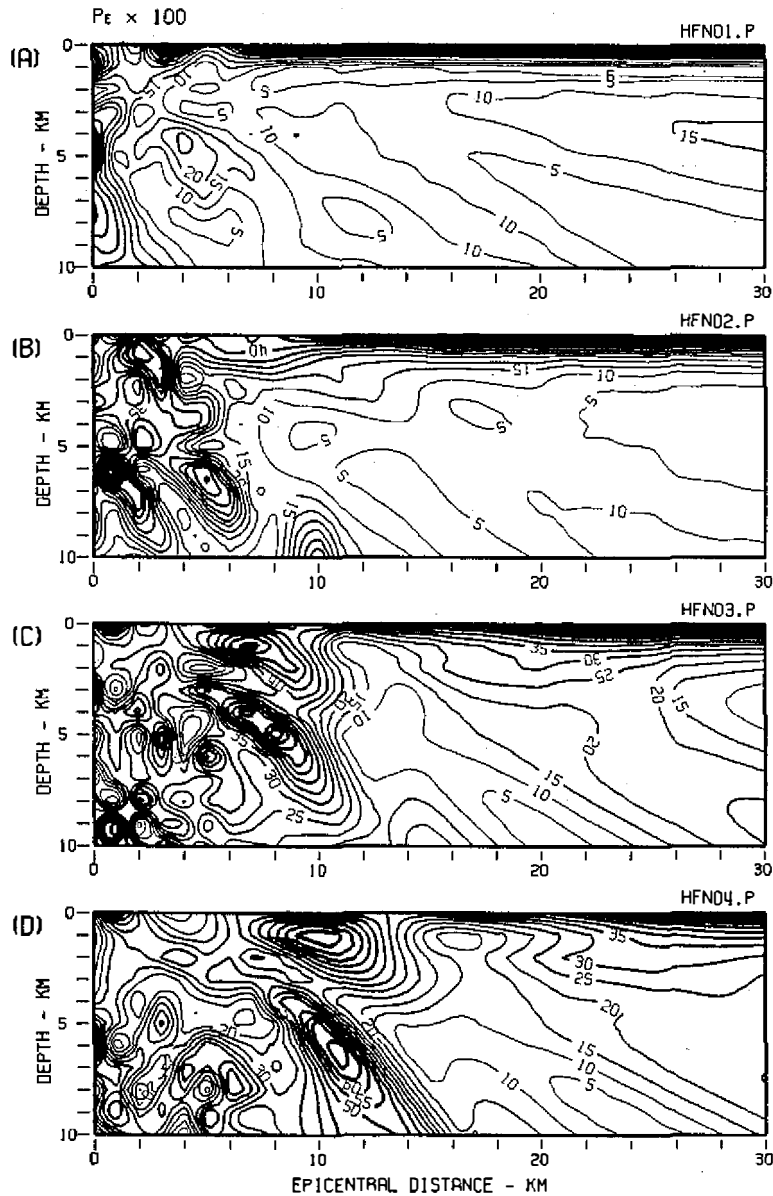


Fig. 7. The averaged ellipticity variations of particle motions over space for certain wavelet propagating through the different positions of the two-dimensional half-space medium. These diagrams are for (A) 2 km, (B) 4 km, (C) 7 km, and (D) 10 km of 3 km-length source depth respectively. The dip angle of the finite-fault is 45° .

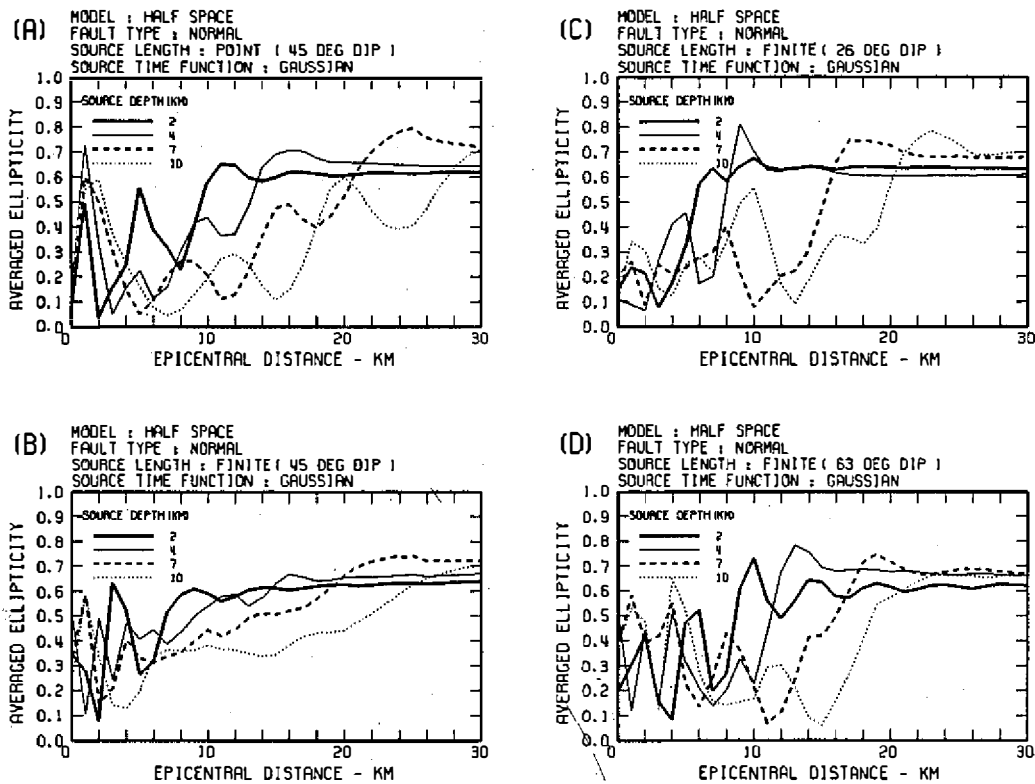


Fig. 8. The variations of the averaged ellipticity of the selected wavelet propagating through the free surface of different distances for the half-space model and (A) point source, (B) 45° - dip, (C) 26° - dip, and (D) 63° - dip finite faults.

characterize this behavior. Besides the contributions from the reflection and refraction phases, the ringing effect due to finite element mesh (Shipley *et al.*, 1967) can also be not regarded as negligible factor. Although the adequate damping matrix has constantly been added over the whole model to attenuate the ringings, the results are nearly the same because the main signals are simultaneously reduced in the same degree at such close distances.

3.2 A Layer Over Half-Space Model

It is well-known that the investigation of surface wave propagation in layered half-spaces is mathematically cumbersome. The physically relevant information, however, is already concealed within a usual period equation obtained by setting a six-order determinant equal to zero (Kuo and Nafe, 1962; Malischewsky, 1987). The semi-analytical and pure numerical methods are more popular from those of earlier studies.

In order to solve such a problem, the dispersive wave groups are evidently distinguishable in our computations. The complicated and large amplitude waveforms are observed since the energy trapped in the surface layer corresponds to the multiple reflections. It's also

shown on the plots that there are several turns implied in every phase arrival in the particle motion orbit. In practice, it is hard to trace one integral wavelet throughout the model because of the influence due to the interface. Alternatively, these authors have chosen the latest and dominant phase propagating with the group velocity of 1.54 km/sec within the top layer. It corresponds to the fundamental mode Rayleigh wave obtained in detail from the Newton-Raphson iteration method under the present conditions (Mooney and Bolt, 1966).

Specific results are given for the different source mechanisms used previously. Figure 9 shows an interesting phenomenon which is that the critical distances are all about 10 km for point dislocation sources located at various depths. Unlike the stable ellipticities obtained beyond the critical distances in the half-space model, it can be interfered by other slow multiples (Figure 10 (a)). The lobe-like elliptic polarizations are also probably produced from the refracted waves of multiples. Although these penetrating waves are relatively weak, the fundamental Rayleigh waves with comparable amplitude near the interface boundary and in the substratum are derived from the Haskell's method (Drake, 1980).

It is to be noticed that there is no study of error analysis in this paper. Basically, it is felt that the possible source of error comes from the constant window length of the selected wavelet. It is difficult to take width dependently corresponding to one wavelength of the phase for every record of node. Since there will be irregular contaminations contained in the target phase, the averaged characteristics of particle motion orbits shown in the figures above, then, do not exactly represent the truth. This is expected to be serious mostly in the near source region where the separation of the waves is implicit.

In order to investigate the effect of the initial slip direction of the dislocation source on the results, the "thrust" type Gaussian pulses also used with no changes of the other parameters. The critical distances for the Rayleigh wave build-up are the same as those for the previous "normal" type sources, even the retrograde particle motion trajectories.

4. CONCLUSIONS

The behaviors of the polarized particle motion for certain wavelets are calculated within a two-dimensional source region to investigate the generation and propagation of short-period Rayleigh waves. The results for the half-space model demonstrate that the critical distances, which the Rayleigh wave should build up well beyond, are equal to 3 to 5 times the depth of the point dislocation sources. These distances are shorter for the finite fault of 3 km in length with various orientations. The ellipticities of the Rayleigh waves observed on free surface are approximately in the range of 0.6 to 0.7, but in the meantime quickly decay with depth. The particle motions near the depth of about 1 km are linearly polarized. They could be identified as the fundamental modes. For a layer over half-space model, the complex patterns of particle motions are observed due to the superpositions of many non-direct waves bounded within the top low-velocity layer. The last and dominant phase propagating with the group velocity of 1.54 km/sec within the top layer is analyzed. The estimated critical distances are about 10 km for various sources. These results imply that the surface waves are generated more efficiently even there is the absence of typical particle motion trajectories. At present, these researchers are simulating some of the irregular structures and analyze the waveforms following the same procedures to isolate the source effect from the systematic analysis. However, some further work still remains to be done in order to understand the effect of structures including the topography on the origination of surface waves.

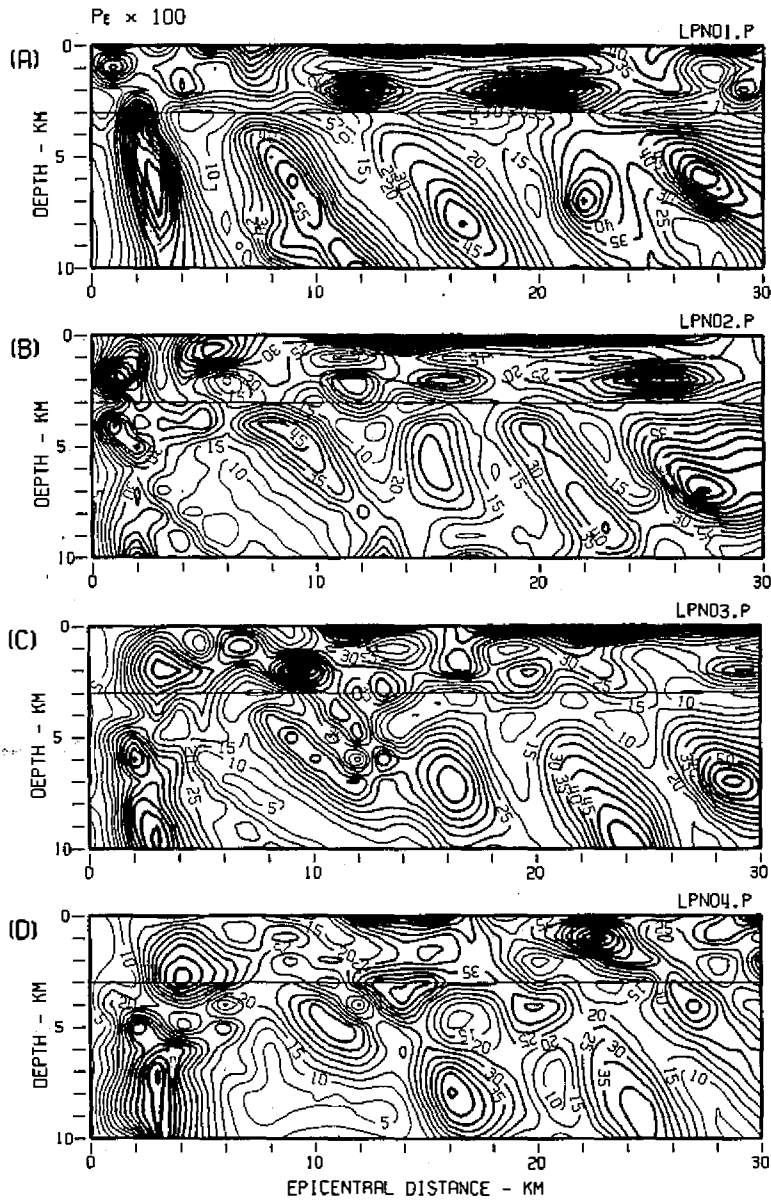


Fig. 9. The averaged ellipticity variations of particle motions over space for certain wavelets propagating through the different positions of a layer over half-space medium. These diagrams are for (A) 2 km, (B) 4 km, (C) 7 km, and (D) 10 km of point source depth respectively. The contour values shown are 100 times the ellipticities.

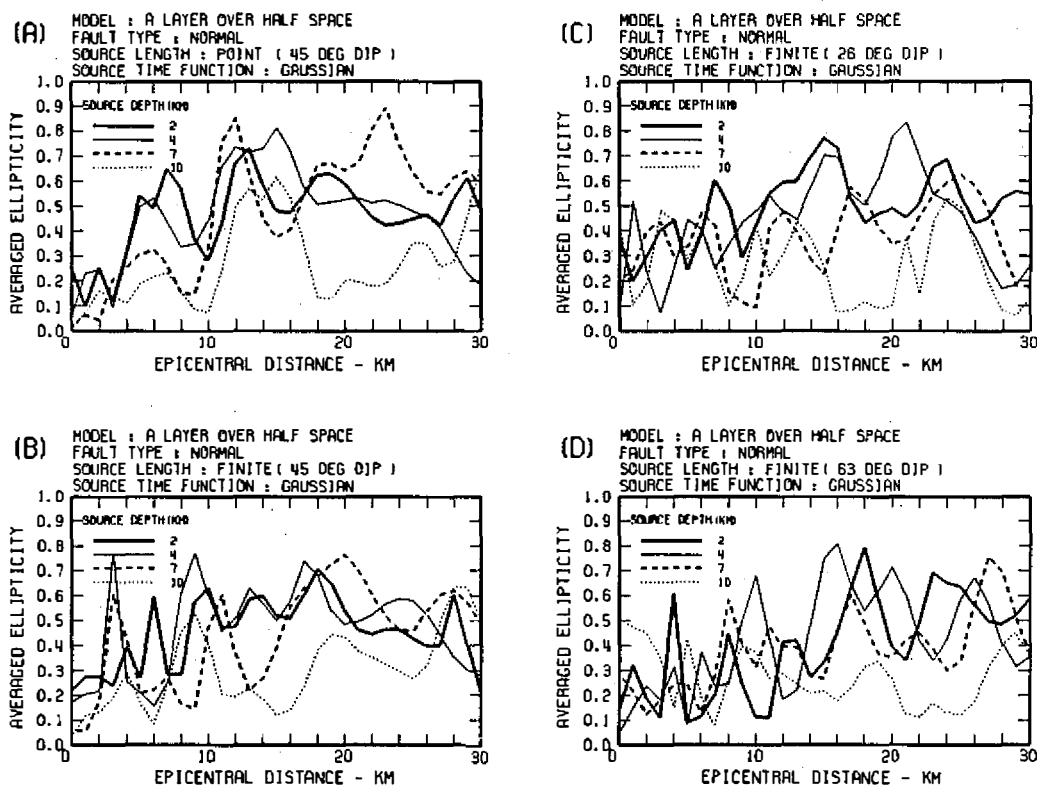


Fig. 10. The variations of the averaged ellipticity of the selected wavelet propagating through the free surface of different distances for a layer over half-space model and (A) point source, (B) 45° - dip, (C) 26° - dip, and (D) 63° - dip finite faults.

Acknowledgements The authors are grateful to Dr. T. C. Shin, Director of the Seismological Observation Center, Central Weather Bureau for providing valuable comments. The authors would like to thank Drs. C. Y. Wang and B. S. Huang for many discussions on the subject. This work was supported by the Central Weather Bureau (CWB81-2E-01).

REFERENCES

- Aki, K., and P. G. Richards, 1980: Quantitative seismology: Theory and methods. W. H. Freeman, San Francisco, 932pp.
- Bard, P.-Y., and M. Bouchon, 1980: The seismic response of sediment filled valley. Part 2. The case of incident P and SV waves. *Bull. Seism. Soc. Am.*, **70**, 1921-1941.

- Bard, P.-Y., M. Campillo, F. J. Chavez-Garcia, and F. J. Sanchez-Sesma, 1988: The Mexico earthquake of September 19, 1985: a theoretical investigation of large and small scale amplification effects in the Mexico City Valley. *Earthquake Spectra*, **4**, 609-633.
- Bath, M., 1973: Introduction to seismology. John Wiley, New York, 395pp.
- Bonamassa, O., and J. E. Vidale, 1991: Directional site resonances observed from aftershocks of the 18 October 1989 Loma Prieta earthquake. *Bull. Seism. Soc. Am.*, **81**, 1945-1957.
- Campillo, M., J. C. Gariel, K. Aki, and F. J. Sanchez-Sesma, 1989: Destructive strong ground motion in Mexico City: source, path and site effects during the great 1985 Michoacan earthquake. *Bull. Seism. Soc. Am.*, **79**, 1718-1734.
- Dorman, J., M. Ewing, and J. Oliver, 1960: Study of shear-velocity distribution in the upper mantle by mantle Rayleigh waves. *Bull. Seism. Soc. Am.*, **50**, 87-115.
- Drake, L. A., 1980: Love and Rayleigh waves in an irregular soil layer. *Bull. Seism. Soc. Am.*, **70**, 571-582.
- Hanks, T. C., and A. G. Brady, 1991: The Loma Prieta Earthquake, ground motion, and damage in Oakland, Treasure Island, and San Francisco. *Bull. Seism. Soc. Am.*, **81**, 2019-2047.
- Hong, T. L., and D. V. Helmberger, 1978: Glorified optics and wave propagation in nonplanar structure. *Bull. Seism. Soc. Am.*, **68**, 1313-1330.
- Hough, S. E., R. D. Borchardt, P. A. Friberg, R. Busby, E. Field, and K. H. Jacob, 1990: The role of sediment-induced amplification in the collapse of the Nimitz freeway during the October 17, 1989 Loma Prieta earthquake. *Nature*, **344**, 853-855.
- Huang, B. S., 1989: Modeling seismic source geometry and rupture processes by finite element method. Ph. D. Thesis, National Central University, Taiwan, 136pp. (in Chinese).
- Kafka, A., and M. Dollin, 1985: Constraints on lateral variation in upper crustal structure beneath southern New England from dispersion of Rg waves. *Geophys. Res. Lett.*, **12**, 235-238.
- Kanamori, H., and J. W. Given, 1981: Use of long-period surface waves for rapid determination of earthquake-source parameters. *Phys. Earth Planet Inter.*, **27**, 8-31.
- Keilis-Borok, V. I., 1989: Seismic surface waves in a laterally inhomogeneous earth. Kluwer Academic Publishers, 294pp.
- Knopoff, L., 1972: Observation and inversion of surface-wave dispersion. *Tectonophysics*, **13**, 497-519.
- Kuo, J. T., and J. E. Nafe, 1962: Period equation for Rayleigh waves in a layer overlying a half space with a sinusoidal interface. *Bull. Seism. Soc. Am.*, **52**, 807-822.
- Malischewsky, P., 1987: Surface waves and discontinuities, Developments in solid Earth geophysics. Vol. 16., Elsevier, New York, 229pp.
- Melosh, H. J., and A. Raefsky, 1981: A simple and efficient method of introducing faults into finite element calculations. *Bull. Seism. Soc. Am.*, **71**, 1391-1400.
- Mendiguren, J. A., 1977: Inversion of surface wave data in some mechanism studies. *J. Geophys. Res.*, **82**, 889-894.

- Montalbetti, J. F., and E. R. Kanasewich, 1970: Enhancement of teleseismic body phases with a polarization filter. *Geophys. J. R. Astr. Soc.*, **21**, 119-129.
- Mooney, H. M., and B. A. Bolt, 1966: Dispersive characteristics of the first three Rayleigh modes for a single surface layer. *Bull. Seism. Soc. Am.*, **56**, 43-67.
- Phillips, W. S., S. Kinoshita, and H. Fujiwara, 1993: Basin-induced Love waves observed using the strong-motion array at Fuchun, Japan. *Bull. Seism. Soc. Am.*, **83**, 64-84.
- Rial, J. A., and H. Ling, 1992: Theoretical estimation of the eigenfrequencies of 2-D resonant sedimentary basins: numerical computations and analytic approximations to the elastic problem. *Bull. Seism. Soc. Am.*, **82**, 2350-2367.
- Sexton, J. L., A. J. Rudman, and J. Mead, 1977: Ellipticity of Rayleigh waves recorded in the Midwest. *Bull. Seism. Soc. Am.*, **67**, 369-382.
- Shieh, C. F., and R. B. Herrmann, 1990: Ground roll: rejection using polarization filters. *Geophysics*, **55**, 1216-1222.
- Shipley, S. A., H. G. Leistner, and R. E. Jones, 1967: Elastic wave propagation: a comparison between finite element predictions and exact solutions. Proc. of international symposium on wave propagation and dynamic properties of earth materials, 509-519, University of New Mexico Press, Albuquerque.
- Singh, S. K., E. Mena, and R. Castro, 1988: Some aspects of the source characteristics and the ground motion amplifications in and near Mexico City from the acceleration data of the September, 1985, Michoacan, Mexico earthquake. *Bull. Seism. Soc. Am.*, **78**, 451-477.
- Smith, I. M., 1982: Programming the finite element method with application to geomechanics. John Wiley & Sons, New York, 351pp.
- Smith, W. D., 1974: A nonreflecting plane boundary for wave propagation problems. *J. Comp. Phys.*, **15**, 492-503.
- Vidale, J. E., 1986: Complex polarization analysis of particle motion. *Bull. Seism. Soc. Am.*, **76**, 1393-1405.
- Wang, J. H., and F. T. Wu, 1989: Numerical particle motion of Rayleigh waves in laterally inhomogeneous media. *J. Phys. Earth*, **37**, 325-343.
- Yan, B., and S. S. Alexander, 1990: Source mechanism study of the 1982 New Brunswick, Canada, Earthquake sequence using combined surface-wave methods. *Bull. Seism. Soc. Am.*, **80**, 296-312.
- Yao, P. C., and J. Dorman, 1992: Short-period surface-wave dispersion and shallow crustal structure of central and eastern Tennessee. *Bull. Seism. Soc. Am.*, **82**, 962-979.